Accelerated interleaved spiral-IDEAL imaging of hyperpolarized ^{129}Xe for parametric gas exchange mapping in humans

Brandon Zanette and Giles Santyr

Accelerated Interleaved Spiral-IDEAL Imaging of Hyperpolarized ^{129}Xe for Parametric Gas Exchange Mapping in Humans

Brandon Zanette[1,2], Giles Santyr[1,2]

1. Department of Medical Biophysics, University of Toronto, Toronto, ON
2. Translational Medicine Program, Peter Gilgan Centre for Research and Learning, The Hospital for Sick Children, Toronto, ON

In preparation as a Note for **Magnetic Resonance in Medicine**

January 22, 2018
Revision 2

Running Head: Accelerated Spiral-IDEAL Parametric Gas Exchange Mapping

Keywords: Hyperpolarized ^{129}Xe, Gas Exchange, Spiral-IDEAL, MOXE

Correspondence to:
Brandon Zanette
Peter Gilgan Centre for Research and Learning,
The Hospital for Sick Children,
Toronto, ON, Canada,
686 Bay St.
M5G 0A4
Email: brandon.zanette@sickkids.ca
Phone: (416)-813-7654 ext: 307937

MRM Note:
Abstract Word Count =227/250
Main Body Word Count =2784/2800
Figure + Table Count = 4 + 1 = 5/5

ABSTRACT

Purpose: To demonstrate the feasibility of mapping gas exchange with single breath-hold hyperpolarized (HP) ^{129}Xe in humans, acquiring parametric maps of lung physiology. The potential benefit of acceleration using parallel imaging for this application is also explored.

Methods: Six healthy volunteers were scanned with a modified spiral-IDEAL sequence to acquire gas exchange-weighted images using a single dose of ^{129}Xe. These images were fit with the model of xenon exchange (MOXE) on a voxel-wise basis calculating parametric maps of lung physiology, specifically: air-capillary barrier thickness (δ), alveolar septal thickness (d), capillary transit time (t_x), pulmonary hematocrit (HCT), and alveolar surface area-to-volume ratio (SVR). An accelerated version of the sequence was also tested in subset of four volunteers and compared to the fully-sampled (FS) results.

Results: Mean image-wide values calculated from MOXE parametric maps derived from FS dissolved ^{129}Xe spiral-IDEAL images were: δ=0.89±0.17μm, d=7.5±0.5μm, t_x=1.1±0.2s, HCT=28.8±2.3%, and SVR=140±16cm^{-1}, in good agreement with previously published values based on whole-lung spectroscopy of healthy human subjects. Parallel imaging sufficiently reduces artifacting in accelerated images, but increases disagreement with MOXE parameters derived from FS data with mean voxel-wise relative differences of: δ=39±9%, d=22±3%, t_x=117±43%, HCT=11±2%, and SVR=31±12%.

Conclusion: Dissolved HP ^{129}Xe spiral-IDEAL imaging for gas exchange mapping is feasible in humans using a single breath-hold. Accelerated gas exchange mapping is also shown to be feasible, but requires further improvements to increase quantitative accuracy.

INTRODUCTION

Pulmonary MRI using hyperpolarized (HP) ^{129}Xe has advanced considerably in recent years. HP ^{129}Xe MRI has seen use for imaging of obstructive diseases such as asthma, cystic fibrosis (CF), and chronic obstructive pulmonary disease (COPD) (1–4). This technique exploits the ~10^5 increase in signal intensity to visualize the pulmonary airspaces (5). Furthermore, ^{129}Xe has relatively high solubility in the lung parenchyma, blood plasma, and red blood cells (RBCs). As ^{129}Xe dissolves between these tissues, chemical shifts of approximately 197ppm for parenchymal tissue/blood plasma (T/P) and 218ppm for RBCs are exhibited (6). Time-resolved measurements of these signals permit quantification of ^{129}Xe gas exchange between airspaces and lung tissues. Imaging of dissolved ^{129}Xe has the potential to be useful for regional investigation of a variety of diseases affecting gas exchange, which may not be revealed by imaging the airspaces alone. Unfortunately, dissolved ^{129}Xe MRI is inherently challenging due to the small amount of ^{129}Xe dissolved in the lungs at a given instant (1-2% of total ^{129}Xe volume) and short T_2* (~1ms at 3T) (7). Dissolved ^{129}Xe MRI has typically been limited to global spectroscopic methodologies, or indirect observation of gas exchange (8). More recently, with improved hardware and advanced pulse sequences, direct imaging of dissolved ^{129}Xe has become clinically feasible (9–13). However, this is typically limited to regional evaluation of the steady-state magnetization of dissolved ^{129}Xe within a single repetition time (TR) due to the inherent signal challenges discussed above coupled with the added constraints of clinical imaging, specifically single doses of ^{129}Xe and reasonable breath-hold durations (<16s). While steady-state evaluation of ^{129}Xe uptake has been shown to reflect compromised gas exchange, there may be ambiguity regarding the pathophysiological sources of observed signal defects. Imaging weighted to the temporal uptake of ^{129}Xe coupled with modelling of gas exchange may provide new insights into the pathophysiological sources of observed gas exchange dysfunction and improve quantification of impaired lung function with parameters that are more easily comparable between different MRI equipment and sites. Multiple techniques to achieve this are currently being explored (14,15).

One such approach for dissolved ^{129}Xe MRI is spiral-IDEAL (16–18). The spiral nature of k-space coverage combined with IDEAL decomposition efficiently and rapidly acquires data, generating spectrally-resolved images with relatively few acquisitions. This allows for repeated imaging to weight the image signal to ^{129}Xe uptake, thereby permitting parametric mapping of gas exchange (19). However this subsequently lengthens the scan duration, potentially conflicting with

breath-hold requirements. Parallel imaging acceleration with multi-channel receivers has previously been demonstrated with HP ^{3}He MRI (20), and may provide the necessary flexibility to reduce the number of acquisitions required for parametric gas exchange mapping in humans.

In this feasibility study, we demonstrate imaging of dissolved ^{129}Xe uptake with interleaved spiral-IDEAL in healthy humans in a single breath-hold. Gas exchange-weighted images are acquired and fit with the model of xenon exchange (MOXE), calculating parametric maps of important alveolar physiology, including air-capillary barrier thickness (δ), alveolar septal thickness (d), capillary transit time (t_x), pulmonary hematocrit (HCT), and alveolar surface area-to-volume ratio (SVR) (21). These are compared to literature values reported using whole-lung spectroscopy and MOXE in healthy adults. Acceleration and reconstruction using parallel imaging are also demonstrated, exploring the potential benefits and drawbacks for this application.

METHODS

Data Acquisition

Informed written consent from six healthy adults (mean age=29±4years, 3 males, 3 females) was obtained in accordance with the Research Ethics Board at The Hospital for Sick Children. Imaging was performed on a clinical 3T system (Magnetom Skyra, Siemens GmbH, Erlangen, Germany) using a rigid birdcage transmit coil and flexible 8-channel receive array (Rapid Biomedical GmbH, Rimpar, Germany). For spiral-IDEAL imaging, interleaved spiral trajectories (N_{int}=6, FOV=48×48cm^2, matrix=32×32, BW=100kHz) were designed to acquire 2D coronal projections (http://mrsrl.stanford.edu/~brian/vdspiral/). A 410μs hard radiofrequency (RF) pulse was used for excitation, ensuring sufficient gas-phase suppression using side-lobe minima in the frequency domain. Prior to imaging, on-resonance flip angle was measured to be ~25° with a sample of gas on the subject's chest. The transmit frequency was then adjusted to the RBC resonance (218ppm). Gas-phase flip angle was estimated using Bloch simulation to be ~0.5°, yielding sufficient gas signal for normalization without depleting gas-phase magnetization. For spectral encoding, four echo times (TE) with a delay (ΔTE) of 230μs was chosen to maximize the number of signal averages (NSA), while also minimizing T_2* decay. For gas exchange-weighting, the spiral-IDEAL sequence was repeated for five repetition times (TR) (15ms, 25ms, 50ms, 100ms, 200ms). Further pulse sequence details are found in the Supporting Information (Supporting Information Figures S1 and S2). Prior to image acquisition, 23 free induction decays (FIDs) were acquired to measure

the chemical shifts for IDEAL decomposition and bring the dissolved magnetization to a steady-state before imaging (BW=100kHz, 2048 spectral points) resulting in a total scan time of 11s. Four subjects were also scanned with an accelerated version of the fully-sampled (FS) sequence described above. Two-fold acceleration was achieved by prospectively removing every second spiral interleaf shortening the breath-hold duration to 6s. All other parameters were left unchanged to observe the effect on image quality. Enriched xenon (83% ^{129}Xe) was polarized to 10-15% (Model 9800, Polarean, Durham, NC). Xenon doses were calculated based on 10% of total lung capacity (TLC) and balanced with N_2 to a volume of 1L, then inhaled from functional residual capacity (FRC).

Data Analysis

Data were analyzed in MATLAB (MathWorks, Natick, MA). Spectral decomposition of gas, T/P, and RBC data was performed as described by Wiesinger et al. (16). Spiral images were reconstructed using the non-uniform fast Fourier transform algorithm (NUFFT) (22). Images were interpolated to a grid size of 128×128 during reconstruction. For gas exchange mapping, T/P and RBC images were segmented from background based on region of interest (ROI) analysis of the gas-phase images. The segmented images were then normalized by the gas-phase on a voxel-wise basis. For every voxel, normalized T/P and RBC curves were simultaneously fit with MOXE extracting the following fit parameters: normalization constant (b), alveolar barrier-to-septum ratio (δ/d), exchange time constant (T), fraction of ^{129}Xe in blood dissolved in RBCs (η), and capillary transit time (t_x). These parameters were subsequently used to calculate: air-capillary barrier thickness (δ), alveolar septal thickness (d), pulmonary hematocrit (HCT), and alveolar surface-to-volume area (SVR). Assumed constants were: diffusion coefficient of xenon in lung tissue (D=3.3×10^{-10}m^2/s), Ostwald solubilities of xenon in lung tissue (λ=0.2), in plasma (λ_P=0.09), and in RBCs (λ_{RBC}=0.19) (23,24). The MOXE sum of series was truncated after 12 summations. R^2 values for T/P and RBC curve-fitting were calculated parametrically, producing maps describing goodness-of-fit regionally.

For acceleration, the iterative self-consistent parallel imaging reconstruction for arbitrary k-space (SPIRiT) algorithm was used (25) (http://people.eecs.berkeley.edu/~mlustig/Software). A 30×30 region of the centre of k-space of the gas images was used for calibration data. The SPIRiT kernel size was 7×7 for image space reconstruction with 30 iterations. The consistency ratio

between acquired data and calibration was set to 5 based on empirical evaluation of image quality. The accelerated images were analyzed with MOXE as described above with the same segmentation masks used for FS data. Image-wide means ± standard deviations were calculated for each MOXE parameter map and compared to literature. Voxel-wise relative difference maps between the FS and accelerated MOXE parametric maps directly representing lung physiology (δ, *d*, HCT, SVR, t_x) were also calculated in order to assess spatial variation due to acceleration.

RESULTS

Figure 1a shows representative spiral-IDEAL images (TR=200ms) indicating good image quality and spectral decomposition. Accelerated images reconstructed without parallel imaging are shown in Figure 1b. Spiral streaking artifacts are apparent as a result of undersampling. Figure 1c shows accelerated images reconstructed with SPIRiT. These images show suppression of undersampling artifacts, although some streaking in the gas images remains. The accelerated images exhibit decreased signal-to-noise ratio (SNR) compared to the FS images due to the reduced amount of data acquired. Figure 2 shows FS spiral-IDEAL images at all timepoints demonstrating sufficient SNR throughout the imaging experiment. Figure 3 shows the accelerated spiral-IDEAL images reconstructed using SPIRiT. Representative MOXE maps for FS and accelerated datasets are shown in Figure 4ab. Maps of R^2 calculated between the MOXE model and T/P and RBC uptake data are also shown. The FS maps are relatively homogeneous except t_x maps, which were highly variable. Figure 4c shows representative relative difference maps. Table 1 shows study-wide averaged parameters of FS and accelerated maps, including mean unsigned relative differences for MOXE parameters. High relative differences resulting from acceleration were observed in most parameters (>20%) except for HCT which had a study-wide average of 11±2%. Comprehensive results for individual participants can be found in the Supporting Information Tables S1 and S2.

DISCUSSION

This proof-of-concept study demonstrates parametric gas exchange mapping in humans using spiral-IDEAL and MOXE. This represents an important step in clinical translation of regional quantification of lung physiology that has previously shown promise in animals (19,26).

Image-wide estimates of MOXE parameters from FS data averaged across all participants (Table 1) are in reasonably good agreement with previously published global spectroscopic values

(7). However, maps of t_x were highly heterogeneous in this work. Estimating t_x is predominantly determined by the slope of the linear portion of the gas exchange curves, when parenchymal tissue is saturated with ^{129}Xe. Thus, the lack of longer timepoints likely contributed to the high variability observed. The longest timepoint in this work (200ms) is near the transition between the primarily exponential portion (before parenchymal saturation) and the linear portion (after parenchymal saturation) of the uptake curve. Therefore, it is possible that the true trajectory of the uptake slope is difficult to accurately model. This may be addressed by acquiring images with longer delay times, though this comes at the cost of longer breath-holds, further stressing the benefit of acceleration. SVR was observed to be slightly lower, but still within the range reported by Chang et al. (7). This may be due to sensitivity to proper normalization of signals. Consistent calibration of off-resonance gas excitation using hard pulse side-lobe minima remains challenging. This may yield inaccurate calibration of signals between resonances leading to uncertainty in the MOXE normalization parameter, *b*, from which SVR is calculated. This could explain the slightly lower SVR in this study. SVR has also been reported to vary with lung inflation, with lower SVR at TLC than FRC+1L (27). Although subjects inhaled to FRC+1L in this study, it is possible that this inspiration level corresponds to different fractions of a subject's TLC. For parameters affected by lung inflation (i.e. SVR), inspiratory volumes calculated as a fraction of TLC may offer more reproducible quantification (27). Despite these shortcomings, important parameters of δ, *d*, and HCT are within the ranges reported previously by Chang et al. and others investigating alveolar physiology (7,14,28,29).

Acceleration of gas exchange mapping is demonstrated in a subset of participants, reducing the required breath-hold from 11s to 6s, which could be useful for patients with disease who may have difficulty performing extended breath-holds. Alternatively, the time savings could be used to increase the number of sampled gas exchange timepoints and/or allow for volumetric imaging, for example in a stack-of-spirals fashion (30). In this study, acceleration resulted in overall reduced R^2 suggesting worse agreement between the data and MOXE. This introduces bias into the estimation of several parameters. For example, the accelerated study-wide values of t_x and SVR are increased compared to FS estimates. Similarly, acceleration tends to result in an underestimation of *T*, which subsequently yields slightly decreased study-wide averages of δ and *d*. Study-wide averages for other parameters generally agreed with their FS counterparts. Calculated relative difference maps between FS and accelerated physiological parameters (δ, *d*,

HCT, SVR, t_x) exhibit rather high relative differences for the acceleration scheme used. However, HCT appeared to be the parameter most robust to acceleration with a mean study-wide difference of 11±2%. Presumably, the principal causes of disagreement are the reduced SNR and data consistency of the accelerated images due to undersampling and parallel imaging reconstruction. These result in more variable and noisy gas exchange curves contributing to the reduced agreement between the data and MOXE. However, this may be addressed in several ways. Increasing the flip angle will more efficiently utilize the commensurately larger residual magnetization available due to the reduced number of RF pulses/acquisitions in parallel imaging, thereby increasing the SNR and partially compensating for the reduced amount of data collected per image (20). The parallel imaging reconstruction itself may also be improved. SPIRiT has many degrees of freedom which can make optimization complicated, as noted in the original publication (25) and by others (31,32). In this study, SPIRiT parameters were guided by the literature and empirical evaluation of image quality, though further optimization for this application is possible. Additionally, this study likely suffered from suboptimal autocalibration since calibration data came from the centre of undersampled spiral k-space. More robust calibration data could be acquired with variable-density spiral trajectories which are denser and satisfy Nyquist criteria near the centre of k-space, or by appending a fast, fully-sampled scan at a single timepoint to the beginning or end of the sequence. Lastly, the 2× undersampling scheme used may not be practical for the modest acquisition matrix sizes in this study (32×32). More carefully designed undersampling strategies will likely benefit accelerated image quality, trading reduced scan duration for increased parametric mapping accuracy. Future optimization should improve accelerated image quality for this application, thereby increasing the agreement between model and data (R^2) and minimizing disagreement between accelerated FS data.

This feasibility study suffers from other limitations that must be acknowledged. First, this study has a limited number of participants. Imaging of more healthy subjects is required to be certain that physiological estimates extracted using this technique are truly in agreement with previously published data and clinical gold standards (i.e. pulmonary function tests). The imaging in this study is limited to 2D projections, preserving SNR throughout the imaging experiment and keeping the number of acquisitions low to conform to clinical breath-holds. This limits clinical utility by removing volumetric information. Future work will incorporate both volumetric and gas exchange-weighted imaging. However this will likely necessitate acceleration to offset the longer

scan time needed for the increased number of acquisitions required. In-plane spatial resolution in this study was limited to $1.5\times1.5cm^2$. Empirically, we found this balanced readout length with a reasonable number of interleaves. Improved spatial resolution requires increased number of spiral interleaves and/or readout duration of individual interleaves, contributing to increased depletion of the gas-phase magnetization reservoir and T_2*-related signal loss respectively. Improvements to polarization and/or increasing the dose of ^{129}Xe used will improve SNR, permitting 3D imaging and better spatial resolution. Finally, dissolved-phase flip angles were limited to values less than 90° due to transmit voltage limitations as well as SAR restrictions throughout the imaging experiment. Thus the gas exchange-weighting did not achieve complete saturation of dissolved longitudinal magnetization between pulses. This residual magnetization mimics faster ^{129}Xe uptake than truly present, potentially underestimating the fit parameters of T and δ/d. This could explain the slightly lower values of T, d, and δ than previously reported. This was partially offset by bringing the dissolved resonances to a low, steady-state magnetization before imaging begins. Improvements allowing for greater transmit voltage or more sophisticated RF pulse design may allow for saturation pulses in future. Further pulse sequence developments incorporating acceleration may also allow higher flip angles to be used in future without violating SAR restrictions due to the reduced number of acquisitions (and therefore RF deposition). This may also permit the application of a series of moderate flip angle, low bandwidth pulses to the dissolved-phase, saturating dissolved magnetization prior to acquisition. Alternatively, modifications to the model correcting for incomplete saturation may be pursued. Nevertheless, study-wide estimates of FS T, δ/d, d, and δ were within with the ranges previously reported (7).

The technique described in this work has potential as a tool for the investigation of gas exchange dysfunction. This work demonstrates the technical feasibility of implementing this technique in healthy human subjects, allowing for future investigation in patient populations.

CONCLUSION

Parametric mapping of ^{129}Xe gas exchange in humans is feasible using an interleaved spiral-IDEAL acquisition during a single 11s breath-hold in combination with MOXE. Accelerated gas exchange mapping is also shown to be feasible, but requires further improvements to increase quantitative accuracy of MOXE parameters and to realize the full benefit of reduced breath-hold durations.

ACKNOWLEDGMENTS

The authors thank Dr. Marcus Couch, Saidah Hack, Nikhil Kanhere, Elaine Stirrat, Andras Lindenmaier, Yonni Friedlander, Ruth Weiss, Tammy Rayner, Manoj Singh, and Rosie Lye for assistance with imaging experiments. B.Z. was supported by a research training competition award (RESTRACOMP) from The Hospital for Sick Children. Study supported by an NSERC Discovery grant (RGPIN 217015-2013) and a CIHR operating grant (MOP 123431).

REFERENCES

1. Fain SB, Korosec FR, Holmes JH, O'Halloran R, Sorkness RL, Grist TM. Functional lung imaging using hyperpolarized gas MRI. J. Magn. Reson. Imaging [Internet] 2007;25:910–23.
2. Mugler III JP, Altes TA. Hyperpolarized 129Xe MRI of the human lung. J. Magn. Reson. Imaging 2013;37:313–31.
3. Kruger SJ, Nagle SK, Couch MJ, Ohno Y, Albert M, Fain SB. Functional imaging of the lungs with gas agents. J. Magn. Reson. Imaging 2016;43:295–315.
4. Ebner L, Kammerman J, Driehuys B, Schiebler ML, Cadman R V., Fain SB. The role of hyperpolarized 129xenon in MR imaging of pulmonary function. Eur. J. Radiol. [Internet] 2017;86:343–352.
5. Möller HE, Chen XJ, Saam B, Hagspiel KD, Johnson GA, Altes TA, de Lange EE, Kauczor H-U. MRI of the Lungs Using Hyperpolarized Noble Gases. Magn. Reson. Med. 2002;47:1029–51.
6. Sakai K, Bilek AM, Oteiza E, Walsworth RL, Balamore D, Jolesz FA, Albert MS. Temporal dynamics of hyperpolarized 129Xe resonances in living rats. J. Magn. Reson. B 1996;111:300–4.
7. Chang Y V, Quirk JD, Ruset IC, Atkinson JJ, Hersman FW, Woods JC. Quantification of human lung structure and physiology using hyperpolarized 129Xe. Magn. Reson. Med. 2014;71:339–344.
8. Ruppert K, Brookeman JR, Hagspiel KD, Mugler JP. Probing lung physiology with xenon polarization transfer contrast (XTC). Magn. Reson. Med. 2000;44:349–357.
9. Cleveland ZI, Cofer GP, Metz G, et al. Hyperpolarized Xe MR imaging of alveolar gas uptake in humans. PLoS One 2010;5:e12192.
10. Qing K, Ruppert K, Jiang Y, et al. Regional mapping of gas uptake by blood and tissue in the human lung using hyperpolarized xenon-129 MRI. J. Magn. Reson. Imaging 2014;39:346–59.
11. Qing K, Mugler JP, Altes TA, Jiang Y, Mata JF, Miller GW, Ruset IC, Hersman FW, Ruppert K. Assessment of lung function in asthma and COPD using hyperpolarized 129Xe chemical shift saturation recovery spectroscopy and dissolved-phase MRI. NMR Biomed. 2014;27:1490–1501.
12. Kaushik SS, Robertson SH, Freeman MS, He M, Kelly KT, Roos JE, Rackley CR, Foster WM, Mcadams HP, Driehuys B. Single-breath clinical imaging of hyperpolarized 129xe in the airspaces, barrier, and red blood cells using an interleaved 3D radial 1-point Dixon acquisition. Magn. Reson. Med. 2016;75:1434–1443.
13. Wang JM, Robertson SH, Wang Z, et al. Using hyperpolarized 129 Xe MRI to quantify regional gas transfer in idiopathic pulmonary fibrosis. Thorax [Internet] 2018;73:21–28.

14. Kern AL, Gutberlet M, Voskrebenzev A, Klimeš F, Rotärmel A, Wacker FK, Hohlfeld J, Vogel-Claussen J. Mapping of regional lung microsctructural parameters using hyperpolarized 129Xe dissolved-phase MRI in healthy volunteers and patients with chronic obstructive pulmonary disease. Magn. Reson. Med. 2018:E-Pub ahead of print.
15. Kern AL, Gutberlet M, Qing K, et al. Regional investigation of lung function and microstructure parameters by localized129Xe chemical shift saturation recovery and dissolved-phase imaging: A reproducibility study. Magn. Reson. Med. 2018:E-Pub ahead of print.
16. Wiesinger F, Weidl E, Menzel MI, Janich MA, Khegai O, Glaser SJ, Haase A, Schwaiger M, Schulte RF. IDEAL spiral CSI for dynamic metabolic MR imaging of hyperpolarized [1-13C] pyruvate. Magn. Reson. Med. 2012;68:8–16.
17. Doganay O, Wade T, Hegarty E, McKenzie C, Schulte RF, Santyr GE. Hyperpolarized 129 Xe imaging of the rat lung using spiral IDEAL. Magn. Reson. Med. 2016;76:566–576.
18. Doganay O, Chen M, Matin T, Rigolli M, Phillips J, Mcintyre A, Gleeson F V. Magnetic resonance imaging of the time course of hyperpolarized Xe gas exchange in the human lungs and heart. Eur. Radiol. [Internet] 2018:E-Pub Ahead of Print.
19. Zanette B, Stirrat E, Jelveh S, Hope A, Santyr G. Physiological gas exchange mapping of hyperpolarized 129Xe using spiral-IDEAL and MOXE in a model of regional radiation-induced lung injury. Med. Phys. 2018;45:803–816.
20. Lee RF, Johnson G, Grossman RL, Stoeckel B, Trampel R, McGuinness G. Advantages of parallel imaging in conjunction with hyperpolarized helium - A new approach to MRI of the lung. Magn. Reson. Med. 2006;55:1132–1141.
21. Chang Y V. MOXE: A model of gas exchange for hyperpolarized 129Xe magnetic resonance of the lung. Magn. Reson. Med. 2013;69:884–890.
22. Fessler JA, Member S, Sutton BP. Nonuniform Fast Fourier Transforms Using Min-Max Interpolation. IEEE Trans Signal Process. 2003;51:560–574.
23. Ruppert K, Mata JF, Brookeman JR, Hagspiel KD, Mugler JP. Exploring Lung Function with Hyperpolarized 129Xe Nuclear Magnetic Resonance. Magn. Reson. Med. 2004;51:676–687.
24. Ladefoged J, Andersen a M. Solubility of Xenon-133 at 37°C in Water, Saline, Olive Oil, Liquid Paraffin, Solutions of Albumin, and Blood. Phys. Med. Biol. 1967;12:307.
25. Lustig M, Pauly JM. SPIRiT: Iterative self-consistent parallel imaging reconstruction from arbitrary k-space. Magn. Reson. Med. 2010;64:457–471.
26. Doganay O, Stirrat E, McKenzie C, Schulte RF, Santyr GE. Quantification of regional early stage gas exchange changes using hyperpolarized 129Xe MRI in a rat model of radiation-induced lung injury. Med. Phys. [Internet] 2016;43:2410–2420.
27. Stewart NJ, Horn FC, Norquay G, Collier GJ, Yates DP, Lawson R, Marshall H, Wild JM. Reproducibility of quantitative indices of lung function and microstructure from 129Xe chemical shift saturation recovery (CSSR) MR spectroscopy. Magn. Reson. Med. 2017;77:2107–2113.
28. Stewart NJ, Leung G, Norquay G, et al. Experimental validation of the hyperpolarized 129Xe chemical shift saturation recovery technique in healthy volunteers and subjects with interstitial lung disease. Magn. Reson. Med. 2015;74:196–207.
29. Ruppert K, Qing K, Patrie JT, Altes TA, Mugler JP. Using Hyperpolarized Xenon-129 MRI to Quantify Early-Stage Lung Disease in Smokers. Acad. Radiol. [Internet] 2018:E-Pub Ahead of Print.
30. Zanette B, Santyr G. Clinical Translation of 3D Spiral-IDEAL for Single Breath-hold Imaging of Gas and Dissolved-Phase Hyperpolarized 129Xe in Human Lungs. Proc. Intl. Mag. Reson. Med. 2018;26:4469.

31. Wright KL, Hamilton JI, Griswold MA, Gulani V, Seiberlich N. Non-Cartesian parallel imaging reconstruction. J. Magn. Reson. Imaging 2014;40:1022–1040.
32. Chang Y V., Vidorreta M, Wang Z, Detre JA. 3D-accelerated, stack-of-spirals acquisitions and reconstruction of arterial spin labeling MRI. Magn. Reson. Med. 2017;78:1405–1419.

TABLES

Table 1: Mean MOXE gas exchange parameters calculated across all fully-sampled (FS) subjects (N=6) and subjects scanned with accelerated sequence (N=4). Parametric evaluation of fit to model (R^2) for T/P and BC gas exchange curves is also included. Previously reported MOXE values in humans (N=10) using global spectroscopy are included for comparison (7).

	Spiral-IDEAL			Literature
Parameter	**Fully-Sampled**	**Accelerated**	**Relative Difference (%)**	
b	0.0101±0.0006	0.0101±0.0006	-	0.019±0.004
δ/d	0.12±0.02	0.12±0.03	-	0.11±0.03
T(ms)	18±2	12±1	-	26±13
η	0.46±0.03	0.47±0.04	-	0.43±0.07
t_x(s)	1.1±0.2	1.6±0.3	117±43	1.3±0.3
δ(μm)	0.89±0.17	0.73±0.20	39±9	1.0±0.3
d(μm)	7.5±0.5	6.1±0.3	22±3	9.2±6.5
HCT(%)	28.8±2.3	29.7±3.2	11±2	27±50
SVR(cm^{-1})	140±16	170±17	171±12	210±50
T/P R^2	0.76±0.03	0.66±0.05	-	-
RBC R^2	0.66±0.07	0.50±0.10	-	-

Values reported represent the aggregate mean ± standard deviation of all image-wide means calculated across all subjects in this study. Relative difference is calculated as the mean of 100%× |Accelerated-FS|/FS for each voxel in an image averaged across all subjects in the study.

FIGURES

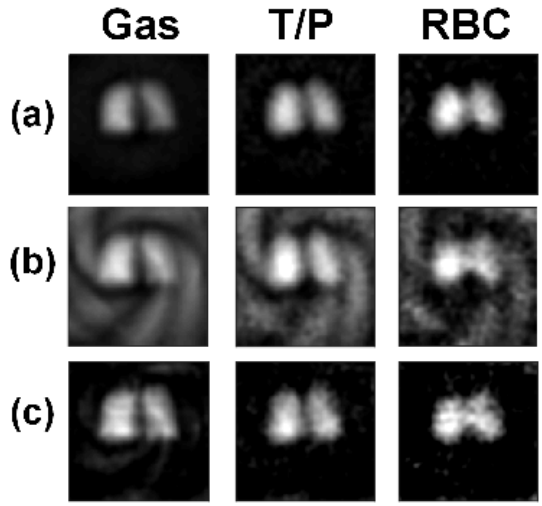

Figure 1: Representative spiral-IDEAL images (200ms) from a single subject. **(a)** Fully-sampled and reconstructed images. **(b)** Undersampled images reconstructed without parallel imaging. Images exhibit severe spiral artifacting, especially in the gas image. **(c)** Undersampled images reconstructed with SPIRiT. Some spiral streaking is still apparent in the gas images; however most artifacting is removed from the T/P and RBC images.

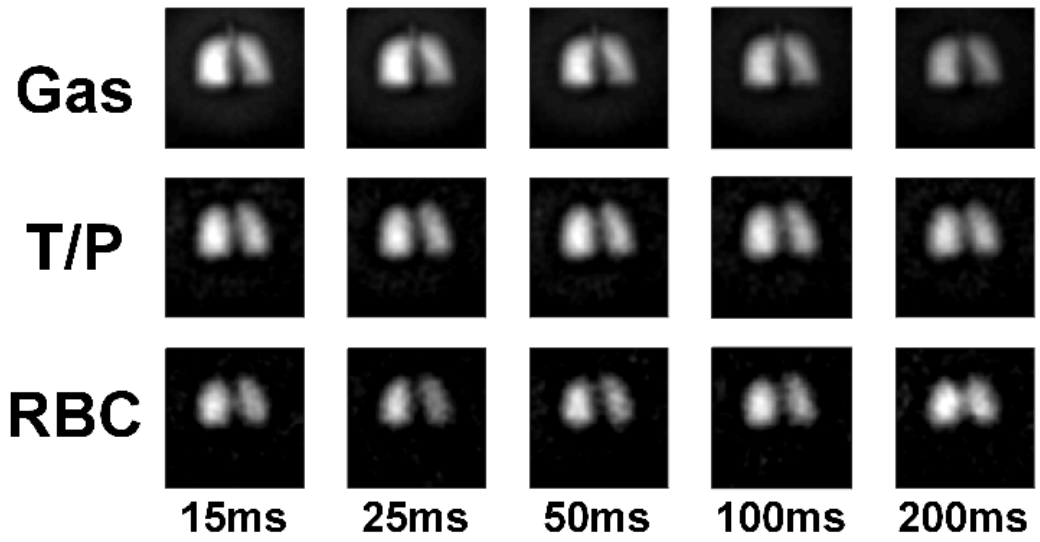

Figure 2: Representative fully-sampled spectrally decomposed spiral-IDEAL images from all acquired gas exchange timepoints. Entire dataset acquired in an 11s breath-hold.

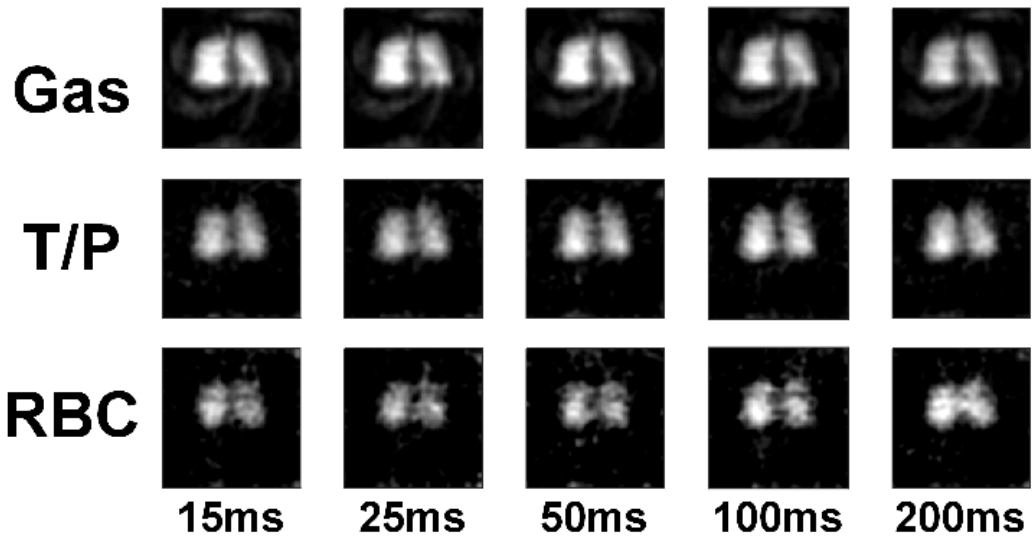

Figure 3: Accelerated spiral-IDEAL images reconstructed with SPIRiT at all timepoints from the same subject as Figure 2. Accelerated data acquired in a reduced breath-hold of 6s duration.

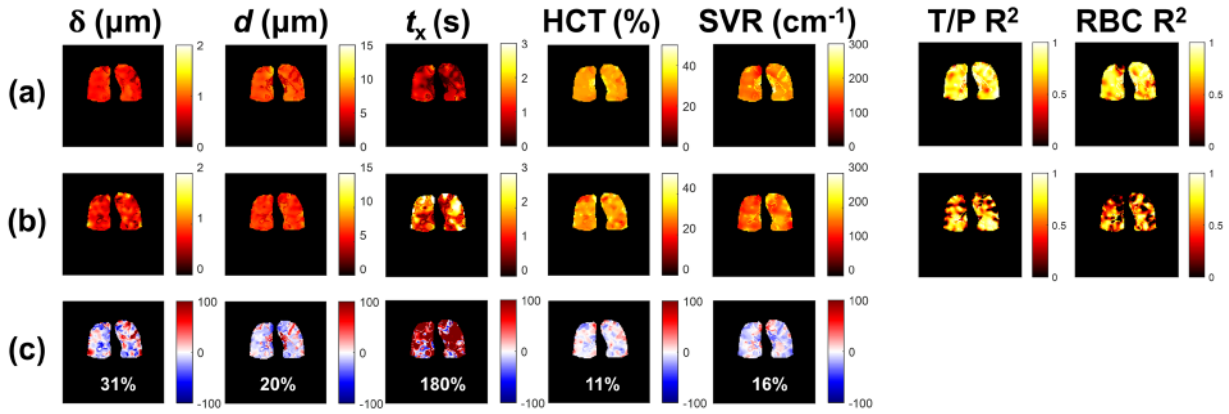

Figure 4: Representative parametric MOXE maps of human lung physiology and R^2 goodness of fit for T/P and RBC curves. **(a)** Results from fully-sampled (FS) dataset from a healthy volunteer. **(b)** Results from an accelerated scan and analysis in the same volunteer. **(c)** Relative difference maps between FS and accelerated data in percent (colormaps capped at ±100%). White text shows absolute image-wide mean of the relative difference maps.